

# Positional-Encoding Image Prior

Nimrod Shabtay\*, Eli Schwartz\*, Raja Giryes  
Tel-Aviv University

## Abstract

In Deep Image Prior (DIP), a Convolutional Neural Network (CNN) is fitted to map a latent space to a degraded image (e.g. noisy) image but in the process learns to reconstruct the clean image. This phenomenon is attributed to CNN’s internal image-prior. We revisit the DIP framework, examining it from the perspective of a neural implicit representation. Motivated by this perspective, we replace the random or learned latent with Fourier-Features (Positional Encoding). We show that thanks to the Fourier features properties, we can replace the convolution layers with simple pixel-level MLPs. We name this scheme “Positional Encoding Image Prior” (PIP) and exhibit that it performs very similarly to DIP on various image-reconstruction tasks with much less parameters required. Additionally, we demonstrate that PIP can be easily extended to videos, where 3D-DIP struggles and suffers from instability. Code and additional examples for all tasks, including videos, are available on the project page [nimrodshabtay.github.io/PIP](https://nimrodshabtay.github.io/PIP).

## 1. Introduction

Deep Image Prior (DIP) [28] has shown that if a CNN is trained to map random noise or a learned latent code to a degraded image, it will either converge to the restored image (e.g. for super-resolution) or produce the restored image in the middle of the optimization process (e.g. for denoising). This has been attributed to an internal image-prior that CNNs have. Even though DIP is used in a zero-shot setup with no supervision and with only a degraded image available, it achieves impressive results for many image restoration tasks, including denoising, super-resolution, inpainting and more. DIP was also extended to other tasks such as segmentation and dehazing using DoubleDIP [8], video processing [36] and 3D mesh reconstruction [11].

Despite the remarkable success of DIP, it is still unclear why fitting random noise to a deteriorated image can restore the image. One explanation to how DIP works, but not why it works, is that the CNN learns to fit first the low frequen-

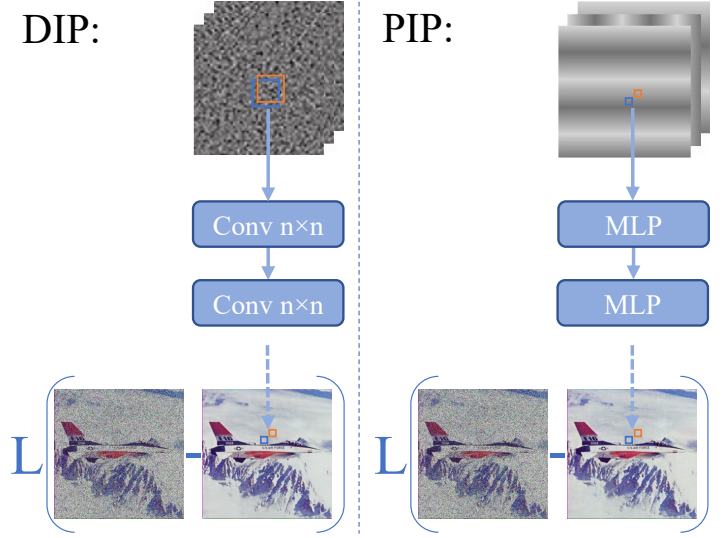


Figure 1. We offer a novel view of DIP as an implicit model that maps noise to RGB values (left). Although it fits noise to produce a degraded image, DIP reaches a clean image. We suggest that this image-prior, or regularization, stems from the fact that neighboring pixels in the output image (blue and orange in the picture) are a function of almost the same noise box in the input but a bit shifted. With this implicit model perspective, we suggest that one may achieve a similar ‘image-prior’ effect by replacing the input noise with Fourier-Features. As a result, we may use a simple pixel-level MLP that has much less parameters than the DIP CNN and still reconstruct images of the same quality. Remarkably, for video this leads to a significant improvement.

cies and only later the higher frequencies, hence early stopping has a low-pass filter effect [25].

In this work, we propose that DIP should be considered as a neural implicit model that is trained to represent the target image. These models gained high popularity in the task of 3D scene representation, due to their use in Neural Radiance Fields (NeRF) [20] and its many follow-ups works. They are also used for 2D image super-resolution [4], but not in the zero-shot form; they learn to map representations from a pre-trained CNN to RGB values.

Neural implicit functions are neural models trained to represent a signal, by training a multilayer perceptron

\*Equal contribution

(MLP) to map the coordinates of the target signal (an image in our case) to the value in these coordinates (RGB color in the case of images). This results in a neural network that implicitly represents the image. It can generate it by simply calculating the output of all its coordinates and even interpolating the image by using a finer grid as input.

Training an implicit model with the raw coordinates as input results in an oversmoothed output due to the spectral bias of neural networks towards low frequencies [23]. To overcome that, it has been shown that by mapping the input coordinates to Fourier-Features, the implicit model can also learn higher frequencies. This leads to a remarkable improvement in the ability of neural implicit representations.

Taking the neural implicit representation perspective, we may think of the inputs of DIP as the equivalent of the coordinate representation in implicit models. With this view in mind, DIP maps random codes to RGB values. However, despite the initial impression, this is not totally a random code. Providing independent random codes for each coordinate and then training an implicit neural model using MLP for a given image simply does not work. Yet, due to the convolutional structure of DIP, there is a “structure” in the randomness. The encoding for a specific location in the image is a shifted version of the random codes of its neighbouring coordinates. Thus, DIP can be considered as an implicit function that maps shifted random codes of the coordinates to the RGB values of the target image. With this view in mind, a natural question is why not simply use other types of positional-encodings for the input coordinates? Or more specifically, Fourier features, which have been proven to be successful for neural implicit representation.

We refer to this setup of DIP with positional-encoding inputs as “Positional-Encoding Image Prior” (PIP). PIP outperforms DIP on an array of tested image-restoration tasks, including denoising, super-resolution, and inpainting. Moreover, we show that using Fourier features the convolutional layers in the DIP architecture can be replaced by an MLP (or  $1 \times 1$  conv.) operating independently on each coordinate. The MLP-based architecture is inspired by the MLP used for implicit models, but it is not identical as we still have skip-connection and down/up-sampling like in the original DIP. This allows achieving the same and even better performance compared to conventional DIP but with a lower parameter count and FLOPS.

A remarkable advantage of PIP is that it can easily be adapted to other modalities, such as video (3D), by modifying its encoded dimensions. In contrast, extending DIP to video by employing random input encoding with 3D convolutions (3D-DIP) struggles to give reliable results. PIP, on the other hand, achieves high-quality reconstruction and significantly outperforms 3D-DIP for video tasks using a simple extension of the 2D PIP to 3D and using Fourier features that encode both the spatial and temporal dimensions.

## 2. Related Work

**Positional encoding** was first presented in the transformer architecture [29], where the importance of positional encoding in learning without an explicit structure was demonstrated. The visual transformer (ViT) [6] extended the transformer architecture along with the concept of positional encoding to the 2D visual domain, where an image is broken into patches and each patch contains the pixel values along with their corresponding spatial location in the image. Peiris et al. [21] used Fourier-features as the positional encoding of transformers for achieving accurate segmentation masks in medical imaging applications.

Another area of research utilizing positional encoding is implicit neural functions, which are neural networks optimized to map input coordinates to target values. It was demonstrated in [27] that representing the input coordinates as Fourier-features with a tuneable bandwidth enables a simple MLP to generate complex target domains such as image and 3D shape while preserving their high level of detail. In Neural radiance fields (NeRF) [20] implicit functions with Fourier features are used for synthesizing novel views of a 3D scene from sparse 2D images. SIREN [26] showed that by changing the activation function of a simple MLP to a periodic one, the network can represent the spatial and temporal derivatives so one can use a regular grid of input coordinates to successfully recover a wide range of target domains (images, videos, 3D surfaces, etc.). Local implicit image functions (LIIF) [4] represent an image as a continuous function using an implicit model. This allowed it to perform super-resolution at an arbitrary scale. Xu et al. [31] show how positional encoding can be interpreted as a spatial bias in GANs. SAPE [13] and BACON [17] demonstrate how a combination of a coordinate network along with a limitation of its frequency spectrum can achieve a multi-scale representation of the target domain.

Due to the success of implicit models, coded by Fourier-features, other areas of research incorporate Fourier-features representation. For example, Li et al. [15] apply learned Fourier-features to control the inputs to gain better sample efficiency in many reinforcement learning problems. Bustos-Brinez et al. [2] use random Fourier-features to perform accurate data-set density estimation for anomaly detection. In this work, we treat DIP as an implicit model and show that as such it can be used with FF and a MLP.

**Deep Image Prior (DIP)** [28] showed that a CNN network (typically a U-net shaped architecture) can recover a clean image from a degraded image in the optimization process of mapping random noise to a degraded image. The power of DIP is shown for several key image restoration tasks such as denoising, super-resolution and inpainting.

DIP was extended to various applications. Double-DIP [8] introduced a system composed of several DIP networks, where each learns one component of the image such that

their sum is the original image. It has been used for image dehazing and foreground/background segmentation. Self-Deblur [24] performed blind image deblurring by simultaneously optimizing a DIP model and the corresponding blur kernel. In the medical imaging domain several works tried to utilize the power of image priors to reconstruct PET images [9, 10, 12, 32]. Other works tried to improve the performance of image priors using modifications and additions to the original setup. Mataev et al. [19] and Fermanian et al. [7] combined DIP with the plug-and-play framework to improve DIP’s performance in several inverse problems. Zukerman et al. [37] showed how the back-projection fidelity term can improve DIP performance in restoration tasks like deblurring. In other areas, Kurniawan et al. [14] proposed a method for demosaicing based on DIP. Chen et al. [5] suggested DIP-based neural architecture search.

Many other works [3, 25, 30] analyzed DIP and attempted to overcome its limitations, e.g., its spectral bias and the need for early-stopping. These works, however, did so by maintaining the input as a random latent code, focusing on the limitations of the architecture itself. We challenge the use of random input for DIP and aim at improving its lack of robustness when changing the used neural architecture or the target domain, e.g., video.

Chen et al. [36] utilized DIP for large hole inpainting to remove objects from videos. Yet, naively scaling DIP to videos by replacing 2D with 3D convolutions (3D-DIP) fails to maintain temporal consistency. Thus, they introduced additional regularization and inputs to improve temporal consistency issues. Yoo et al. [33] introduced Time-dependent DIP in MRI images, which encodes the temporal variations of images with a DIP network that generates MRI images. Lu et al. [18] utilize DIP for video editing and manipulation. The above works show clearly that DIP cannot be naively extended from images to video and it requires additional regularization and loss functions. On the other hand, PIP can be easily extended to videos. It learns temporal connections and preserves consistency between frames in a controllable and intuitive manner.

### 3. Positional-Encoding Image Prior (PIP)

DIP [28] demonstrates that an untrained CNN generative model can be fitted, in a zero-shot manner, to generate a corrupted image, yet, it eventually will recover the clean image without using explicit regularization. Formally, we have  $x = f_\theta(z)$ , where  $f_\theta$  is a neural network that maps random input codes  $z \in \mathbb{R}^{C \times W \times H} \sim U(0, \frac{1}{10})$  to image space  $x \in \mathbb{R}^{3 \times W \times H}$ . Given a corrupted image  $x_0$ , we want to recover its original clean image. Such an image reconstruction task can be formulated as an energy minimization problem

$$x^* = \operatorname{argmin}_x E(x; x_0) + R(x), \quad (1)$$

where  $E(x; x_0)$  is the data term and  $R(x)$  is a regularization term. The main observation in DIP is that due to the CNN’s image-prior the regularization term can be dropped and the data term can be optimized by adapting the model parameters with gradient-descent

$$\theta^* = \operatorname{argmin}_\theta E(f_\theta(z); x_0), \quad x^* = f_{\theta^*}(z). \quad (2)$$

As illustrated in Fig. 1, one may consider DIP as an implicit model and the random input as a positional encoding of shifted random patches. Thus, in PIP, we suggest replacing the random input codes  $z$  with Fourier-features as the positional-encoding of the image coordinates. Fourier-features are used for positional-encoding in both transformer architectures [6] and implicit models [27]. They have the advantage of being smooth, continuous, and with a controllable bandwidth. For a coordinate vector  $\mathbf{v}$  and set of frequencies  $\{f_0, \dots, f_{m-1}\}$ , the Fourier-features are

$$\gamma(\mathbf{v}) = [\dots, \cos(f_i \mathbf{v}), \sin(f_i \mathbf{v}), \dots]. \quad (3)$$

We use log-linear spaced frequencies  $f_i = \sigma^{i/m}$ , with the base  $\sigma$  set by a predefined maximum frequency, such that  $f_{m-1} = f_{max}$ . Inspired by [16], we also test a learnable-frequencies variant, where the frequencies are initialized as described above and then optimized together with the model parameters using gradient-descent. This variant allows learning the most appropriate encoding to be used for a given image and is beneficial for some tasks.

We further suggest replacing the convolutional layers with MLPs. The intuition is that the PE image-prior is sufficient to make the convolutions redundant. DIP uses an encoder-decoder hourglass architecture. It consists of convolutional layers with strides for down-sampling in the encoder; convolutional layers with simple bi-linear or nearest-neighbors up-sampling in the decoder; and possibly skip connection between corresponding scales in the encoder and decoder. For PIP we adopt the same multi-scale hourglass architecture, but each convolution with  $k \times k$  kernel and  $s \times s$  strides is replaced with a pixel-level MLP followed by nearest-neighbor down-sampling (simply implemented as a convolution with 1 kernel and  $s \times s$  strides). The modifications are described in Fig. 1. The suggested architecture is more efficient in terms of compute and memory:  $1 \times 1$  vs.  $3 \times 3$  convolutions are more efficient in terms of the number of parameters and FLOPs by a factor of 9. In addition, we observe that while DIP is somewhat sensitive to the architecture used (a slightly different architecture is used for each of its tasks), this is not the case for PIP. The same overall architecture works with both convolutions and MLPs, and we use the same architecture for all tested tasks.

Finally, unlike DIP, PIP can be easily adapted to other domains. For example, when DIP is adapted to video (using 3D convolutions), additional losses have to be used to

ensure temporal consistency [33]. In PIP, the model is simply adjusted by defining Fourier features for all dimensions.

**Implementation details.** We follow the original architecture choice of DIP for denoising and SR: 5 levels U-net with skip connections. Each level has 2 convolutional blocks with 128 channels, and the skip connections are with convolutional blocks with 4 channels. We also follow the original DIP hyper-parameters, Adam optimizer with a learning rate of 0.01 and the same number of iterations for early-stopping. For any of the demonstrated applications, we used the original configurations and replaced only the convolutional filters from  $3 \times 3$  to  $1 \times 1$  and plugged in Fourier-features as input instead of noise.

## 4. Evaluations

In this section, we first perform a quantitative evaluation for denoising and super-resolution. We also study the effect of different design choices and understand what makes PIP work from a spectral-bias perspective. We then qualitatively demonstrate the applicability of PIP for more tasks – inpainting and blind-dehazing. In addition to the examples presented in the paper, more examples for all tasks explored can be found on the [project page](#).

We follow the denoising and super-resolution experiments from DIP [28], using the same sets of images. For denoising – 9 colored images<sup>1</sup> with additive Gaussian noise ( $\sigma = 25$ ). For SR – the union of Set14 [35] and Set5 [1], resulting in 19 images, with  $\times 4$  and  $\times 8$  downscaling factors.

As described in Section 3, for each task we tested 4 PIP variants, with CNN vs. MLP architecture and fixed vs. learned frequencies. Table 1 summarizes the results. For detailed comparisons, please see Appendix B for denoising and Appendix C for Super-Resolution. We observe that fixed-frequencies perform slightly better for denoising while learned-frequencies perform slightly better for SR. PIP shows robustness to the architecture used, CNN and MLP have comparable performance, while DIP relies on the CNN and fails with MLP. Figure 2 demonstrates a high correlation in performance between DIP (CNN) and PIP (MLP) suggesting they enjoy similar prior effects. Figures 3 and 4 show examples of the denoising and SR results, respectively, for both PIP and DIP. We observe quite similar generated images, with similar artifacts, suggesting, again, CNN and PE have similar ‘prior’ effect.

**U-Net vs MLP.** DIP employs a U-Net architecture. It has an encoder-decoder structure, where each encoder block uses strides to downsample the image and each decoder block unupsample the image by nearest or bilinear interpolation. Parts of the original resolution signal are passed through skip connections. These downsampling-upsampling operations have the effect of a low-pass filter on the parts of the

	Arch.	Freq.	Denoising	SR $\times 4$	SR $\times 8$
DIP	CNN	-	28.56	28.43	<b>25.01</b>
DIP	MLP	-	20.37	22.04	16.74
PIP	CNN	Fixed	<b>28.80</b>	28.62	24.00
PIP	CNN	Learned	28.28	<b>28.81</b>	24.56
PIP	MLP	Fixed	28.26	28.05	24.26
PIP	MLP	Learned	28.24	28.57	24.76

Table 1. **Denoising and Super-Resolution** datasets evaluation. Compared to DIP-CNN, DIP-MLP fatally fails. On the other hand, PIP is robust to the architecture used and does not require the CNN. Using fixed frequencies is slightly better for denoising, while learned frequencies (optimizing the input frequencies together with model params) are slightly better for SR.

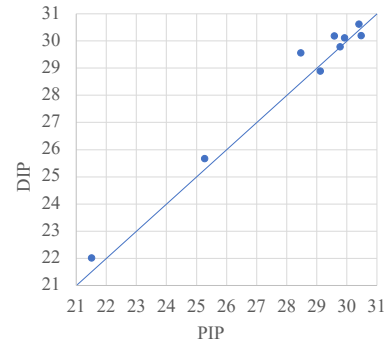


Figure 2. **DIP vs. PIP (MLP) denoising** PSNR for the set of tested images. We observe high correlation. This suggests that PE prior has a similar effect to the convolution prior.

Arch.	Denoising	SR $\times 4$
U-Net MLP	28.26	28.57
Simple MLP	28.42	26.57

Table 2. **The effect of the U-net structure** is evaluated on both the denoising and super-resolution tasks. For denoising, an MLP can perform as well as a multi-scale model like U-Net, but for SR, the multi-scale property has a crucial impact on the results (+2dB)

signal passed through them. This can be treated as part of the image prior of the model. To test this effect we compare  $1 \times 1$  U-Net vs. a simple MLP. Table 2 summarizes the results. It shows that for denoising, a simple MLP, commonly used in implicit models, is enough and performs just as well as the U-Net that operates in a multi-scale scheme. For SR, however, U-Net is much stronger than the simple MLP. This is probably due to the fact that for this task non-local information is important for retrieving the lost high frequencies. Throughout this paper, for the sake of simplicity, we used the  $1 \times 1$  U-Net architecture for all experiments.

**Effect of the Fourier Features (FF) frequency range.** The range of input frequencies allows controlling the generated image. When  $f_{max}$  in FF is too low, we generate a blurry

<sup>1</sup>[https://webpages.tuni.fi/foi/GCF-BM3D/index.html#ref\\_results](https://webpages.tuni.fi/foi/GCF-BM3D/index.html#ref_results)



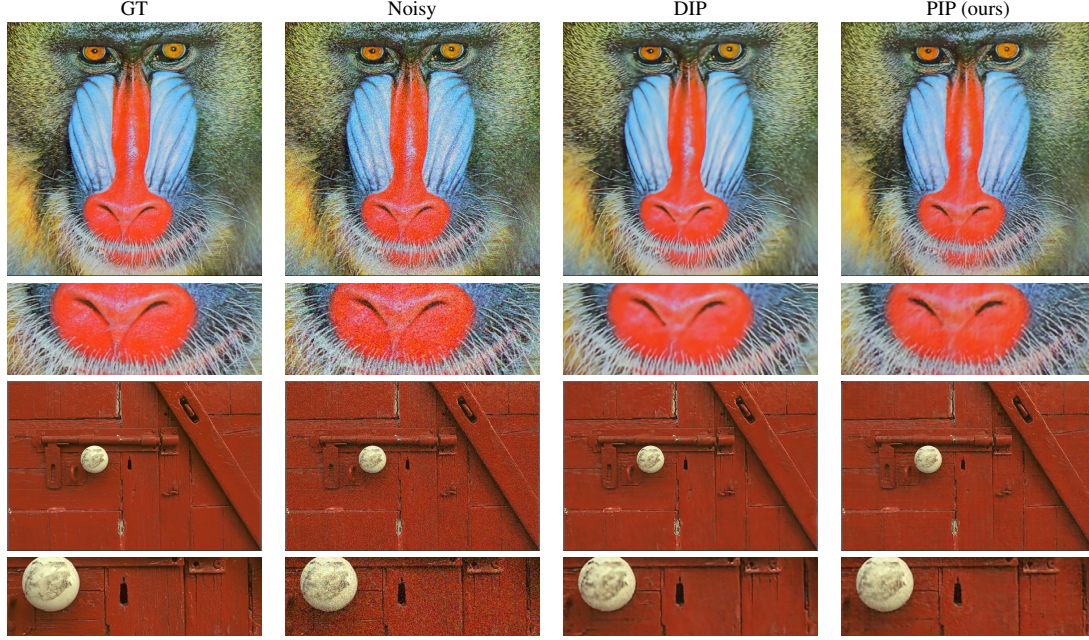


Figure 3. **Image denoising examples** from left to right – the clean image (GT), the noisy image, DIP (CNN) results and PIP (MLP) results. The results for DIP and PIP are very similar, suggesting they have a similar image-prior.



Figure 4. **SR examples** - The first example is for  $\times 4$  SR, the second is for  $\times 8$  SR. The results for DIP (CNN) and PIP (MLP) are very similar, suggesting they have a similar image-prior.

image. When  $f_{max}$  is high we can fit the high-frequency noise. However, thanks to the spectral-bias effect, early-stopping prevents fitting the noise even with high  $f_{max}$ .

Figure 6 demonstrates the effect of  $f_{max}$ . For low  $f_{max} = 2^4$  we get blurry images. We find that  $2^8 \leq f_{max} \leq 2^{10}$  provides a good balance and generates good images. But even if we use the very high  $f_{max} = 2^{16}$ , thanks to the early stopping we still do not fit the noise despite the model capability. We also show the PSNR per-

formance as a function of  $f_{max}$  for the presented image. The performance improves till  $f_{max} = 2^8$ . Then for higher frequencies the performance varies a little bit but with no clear trend of performance degradation.

A special case of limited frequency range is using a “mesh-grid” input, i.e. two input channels containing the horizontal and vertical coordinates. In FF, the encoding with the lowest frequency is  $\sin(x)$ , which simply applies a monotonic mapping to the coordinate and hence produces a

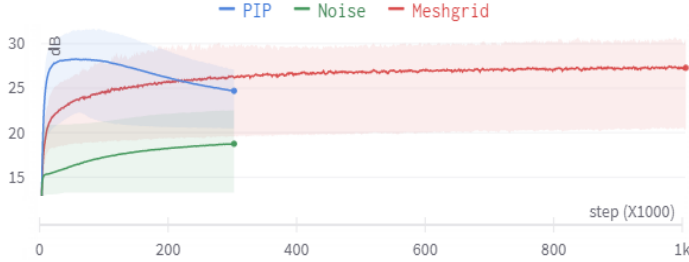


Figure 5. **MLP-Denoising with FF (PIP), Meshgrid and Noise encoding.** Noise encoding fails to generate a valid mapping between the input code and the target image. The meshgrid provides a much better representation but the lack of high frequencies generates an over-smoothed image (see an example 12). PIP lets the model produce a suitable range of frequencies such that it denoises the image well.

Arch.	Params [M]	Train time [sec]
DIP	2.22	160
PIP	<b>0.33</b>	<b>130</b>

Table 3. **Run-time and memory computation** - PIP has 15% of the parameter count compared to DIP, and it’s 18.75% faster during training than DIP

very similar representation. Note that DIP used mesh-grid as input for the inpainting task and in [25] it was tested with a pure MLP. We repeat the experiment here for that task of denoising with the purpose of showing the advantage and the key role of the FF. Figure 5 compares the training of a denoising MLP model with three different options for the input: FF, meshgrid and noise. Clearly, using noise as input with MLP layers does not work (also noted in Table 1). Observe that with meshgrid the model does not overfit and hence does not need early stopping. Yet, it is unable to reach the FF performance even after a long training. This is because it encodes only the lowest frequency, and thus incapable of reconstructing the higher frequencies in the image. See Appendix A for visual examples.

**Computation efficiency.** We compared the original DIP’s CNN vs. our MLP in terms of parameter count and training time for denoising. The number of parameters decreased by a factor of  $\sim 7$  (due to the removal of all spatial filters) and training time decreased by  $\sim 20\%$  (tested on Nvidia 2080TI GPU). Table 3 provides detailed results.

#### 4.1. Spectral Bias

Following [25], which analyzed DIP and showed that the model learns first the low frequencies and then the higher frequencies, we perform a similar evaluation for PIP. To test this, we fit a PIP model to a synthetic image comprised of 3 sinusoidal signals with frequencies  $2\pi \cdot 4, 2\pi \cdot 8, 2\pi \cdot 16$ , while the input range is limited to  $f_{max} = 2\pi \cdot 8$ . Figure 7 presents the synthetic image as well as the generated images during the optimization process. We also display the

Method	Dog	rollerblade	Judo	Camel	Mean
DIP	27.62/0.87	29.4/0.88	31.96/0.92	25.7/0.86	28.67/0.88
3D-DIP	22.23/0.78	25.4/0.84	32.74/0.96	24.407/0.85	26.19/0.86
3D-PIP	<b>28.01/0.89</b>	<b>30.1/0.91</b>	<b>34.78/0.96</b>	<b>25.89/0.86</b>	<b>29.7/0.91</b>

Table 4. Video-Denoising: PSNR/3D-SSIM. 3D-PIP outperforms 2D-DIP (frame-by-frame) and 3D-DIP both in terms of pixel reconstruction (PSNR) and temporal consistency (3D-SSIM).

Fourier transform of the generated images and observe the rate at which the GT delta functions corresponding to the original sinusoidal signals are recovered. We further quantify the convergence during the optimization by measuring the absolute difference between the GT and generated image Fourier transform amplitude for the 3 frequencies (see Figure 8). Clearly, the generated image fits the sinusoidals according to their frequency from smaller to larger.

## 4.2. Additional Applications

We further demonstrate that PIP can serve as a drop-in replacement in other applications DIP is used for.

**Inpainting** We follow the examples demonstrated for DIP. In both cases, we used the learned-FF configuration and increase the number of iterations to  $8k$  instead of  $6k$ . Examples of our inpainting results are presented in Fig. 9.

**Double-PIP - Dehazing** Image dehazing is the problem of extracting a haze-free image from a hazy image. Formally, the image acquisition is modeled as  $I(x) = J(x)t(x) + A(1-t)(x)$  where  $I$  is a hazy image,  $J$  is a haze-free image,  $A$  is the airlight modeling and  $t(x) = e^{-\beta d(x)}$ . In Double-DIP [8], three DIP models are trained together to generate  $J(x)$  and  $t(x)$  ( $A$  can be derived from other algorithms or learned) with respect to the above model. Again we evaluate PIP as a drop-in replacement. We switched all noise inputs to FF and all  $3 \times 3$  conv. layers with  $1 \times 1$  conv. layers. Figure 10 shows that PIP may replace DIP also here.

## 4.3. Extension to Video

### 4.3.1 Video-Denoising

We tested an extension of PIP to video (3D-PIP) on the video denoising task. To that end, we extend our positional encoding from 2D to 3D and encode the temporal domain as well as the spatial domain. Instead of stacking two spatial PEs (one for each coordinate), we stack three PEs (adding a temporal encoding). Since in the case of a video, the model needs to implicitly represent a full video and not a single frame, we increase the model capacity. We change the model to have 6 levels instead of 5 and double the representation depth. An important observation is that other than increasing the model’s capacity, PIP does not use any 3D building blocks (such as 3D convolutional layers or tri-linear interpolation), or any additional loss and regularization as done in [4, 18].



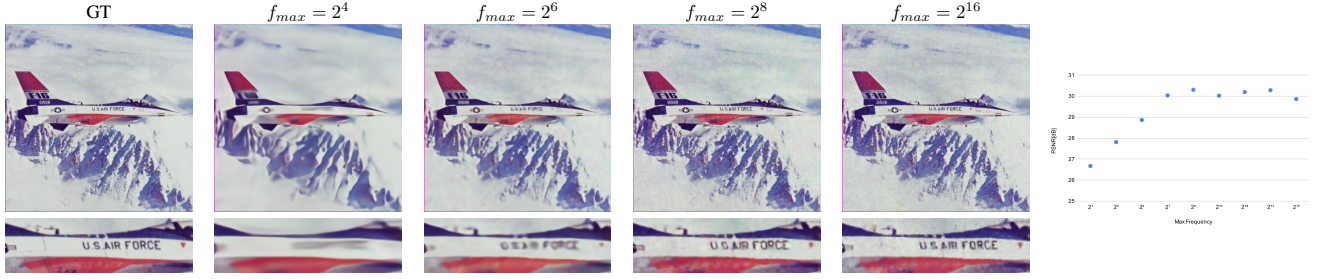


Figure 6. **FF bandwidth** - We compare image denoising results for different  $f_{max}$ . As we increase  $f_{max}$  the reconstruction is sharper until it reach a plateau around  $f_{max} = 2^8$ . Using a very large frequency range,  $f_{max} = 2^{16}$ , does not drastically affect the performance thanks to the role of early-stopping in preventing over-fit to the noise. On the right are the PSNR results as a function of  $f_{max}$ .

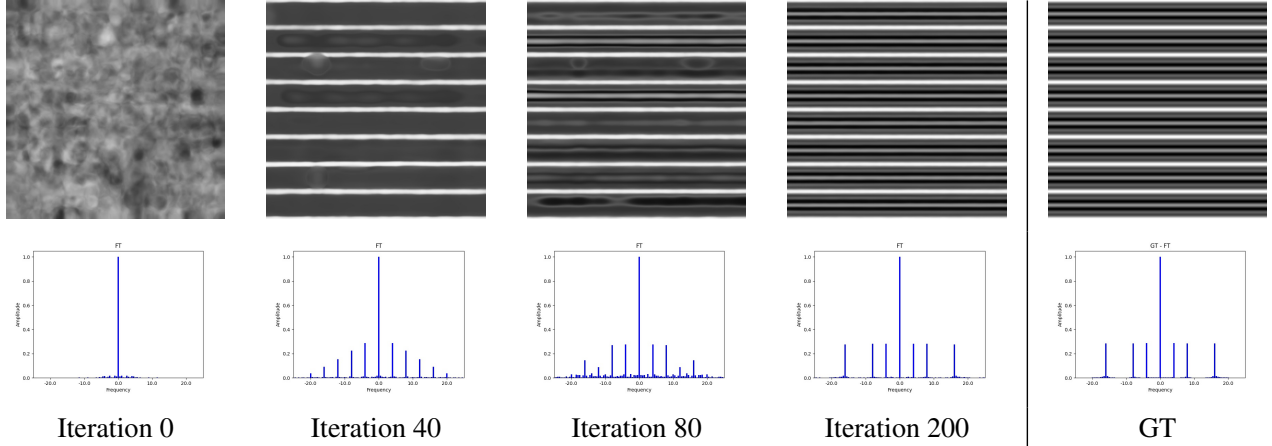


Figure 7. **Spectral Bias** We fit a PIP model to a synthetic image with 3 vertical frequencies (right column). We show the generated images as the training progress (first row) and the Fourier transforms over a vertical line in the image (second row). We find that the model is biased towards first fitting the lower frequencies (lowest frequency at  $\sim 40$  iterations; middle at  $\sim 80$ ; highest at  $\sim 200$ ), see quantitative evaluation of the convergence in Fig. 8. This explains why when the model is early-stopped the image lower frequencies are fitted while the high frequency noise is removed. The highest frequency in the synthetic image is larger than  $f_{max}$  in the model inputs, yet, the model is able to fit it too.

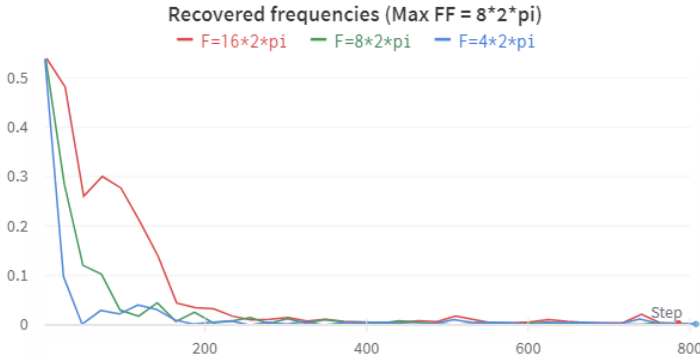


Figure 8. **Spectral Bias**. Quantitative evaluation of the convergence for different frequencies for the synthetic image from Fig. 7. We measure the absolute difference between the predicted frequencies' amplitude vs. the GT amplitudes. Lower frequencies are fitted first during the optimization.

We compare 3D-PIP to two versions of DIP. The first is simply applying 2D-DIP frame-by-frame. The second is

3D-DIP from [4] (adapted for video denoising). We trained all video models for  $5K$  iterations on all frames. We tested them on several videos from the DAVIS dataset [22]. Table 4 summarizes the results for all methods. Figure 11 provides visual examples, links to the generated videos are provided in Appendix D. In addition to PSNR, we also report SSIM-3D [34] to measure temporal-consistency. We can see that 2D-PIP with temporal encoding is better than 3D-DIP by  $4.15dB$  on average PSNR. While frame-by-frame 2D-DIP gets comparable results to 3D-PIP in terms of average PSNR, its lack of consistency is noticeable as reflected in the SSIM-3D score for both 3D-DIP and DIP. Another advantage PIP has over 3D-DIP is that it runs  $\sim 2$  times faster during training.

#### 4.3.2 Video Super-Resolution

In addition to video denoising we also provide results for video spatial SR ( $\times 4$ ) using the same model. The quantitative results are presented in Table 5. Links to the generated

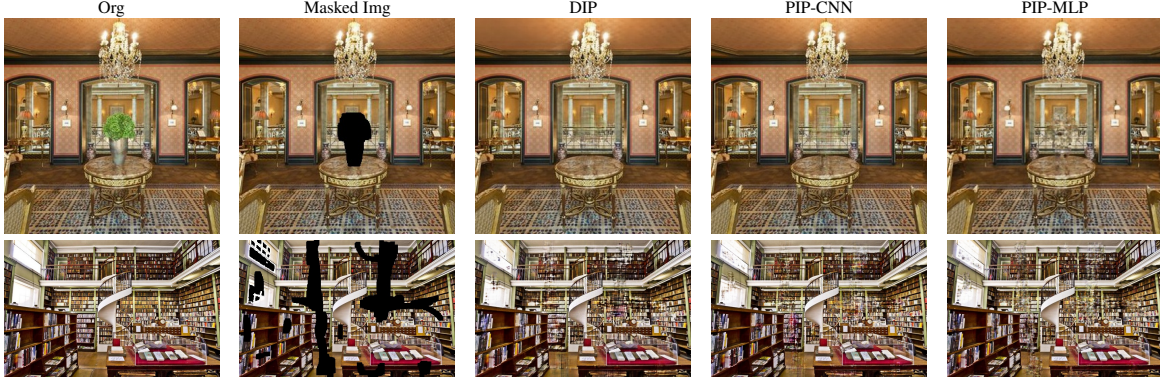


Figure 9. **Image Inpainting.** A comparison on large hole inpainting. PIP-CNN outperforms visually in both images, where PIP-MLP shows comparable results to DIP without any spatial kernels.



Figure 10. **A blind image dehazing example.** We compare “Double-PIP” to “Double-DIP”, where both methods produce comparable visual results.

Method	Dog	rollerblade	Judo	Camel	Mean
DIP (per frame)	26.66/0.87	26.26/0.83	30.26/0.92	24.18/0.83	26.84/0.86
3D-DIP (whole video)	24.27/0.83	24.96/0.80	28.32/0.90	22.74/0.78	25.1/0.83
PIP (whole video)	<b>27.06/0.87</b>	<b>26.93/0.86</b>	<b>31.02/0.94</b>	<b>24.33/0.84</b>	<b>27.33/0.88</b>

Table 5. Video SR: PSNR/3D-SSIM. 3D-PIP outperforms 2D-DIP (frame-by-frame) and 3D-DIP both in terms of pixel reconstruction (PSNR) and temporal consistency (3D-SSIM)

videos are provided in Appendix E. PIP produces higher temporal consistency and less blurry background compared to 2D-DIP (frame-by-frame) and 3D-DIP.

## 5. Conclusions

In this paper we have shed a new light on DIP, treating it as an implicit-model mapping shifted noise-blocks to RGB values. We have shown that Fourier-feature that are popular in implicit models can be used as a replacement for the noise inputs in DIP. Furthermore, when using PE, the convolutional layers can be replaced with MLPs, as commonly done in implicit-models. We showed that the PE’s image-prior is very similar to the CNN’s image-prior, both in terms of quantitative performance (PSNR) and the visual

appearance. Like DIP, we showed that PIP first fits the low-frequencies, providing an explanation on how it operates.

One limitation of PIP is that it uses the same amount of frequencies for all images. An adaptation to the frequencies in a given target image may improve the reconstruction significantly in some cases [13, 17]. In future work, we may explore the selection of the input frequencies based on the input image content, e.g. based on BACON [17]. The frequencies can be also spatially adapted, i.e., different set of frequencies may be employed for different regions in the image as done in SAPE [13]. For example, in the baby image in Fig. 4 it would be beneficial to use lower frequencies for the face and higher for the hat. Smartly choosing the frequencies might also help mitigating another limitation, e.g., the need for early stopping, which is also required for DIP.

Finally, some insights from DIP and PIP might help improving implicit-models, e.g., using multi-scale processing in a U-Net architecture. The PE image-prior we observed might explain the ability of NeRF to interpolate between sparse set of input views. It can also explain the ability of NeRF to learn from noisy inputs, e.g. as exhibited by RAW-NeRF [20]. Our results hint that this ability of NeRF is not just due to averaging samples from different views but also





Figure 11. **Video denoising.** We compare 3D-PIP to 2D-DIP (frame-by-frame) and 3D-DIP (3D conv.). 3D-PIP generates better images (e.g. the grass area) and achieves better temporal consistency (full videos in the sup. material).

due to the impact of PE that generates well-behaved images. Finally, we demonstrated that PIP can be used for higher dimension signals (video denoising), where DIP struggles.

## References

- [1] Marco Bevilacqua, Aline Roumy, Christine Guillemot, and Marie Line Alberi-Morel. Low-complexity single-image super-resolution based on nonnegative neighbor embedding. 2012. 4
- [2] Oscar Bustos-Brinez, Joseph Gallego-Mejia, and Fabio A. González. Ad-dmkde: Anomaly detection through density matrices and fourier features, 2022. 2
- [3] Prithvijit Chakrabarty and Subhansu Maji. The spectral bias of the deep image prior. *CoRR*, abs/1912.08905, 2019. 3
- [4] Yinbo Chen, Sifei Liu, and Xiaolong Wang. Learning continuous image representation with local implicit image function. In *Proceedings of the IEEE/CVF conference on computer vision and pattern recognition*, pages 8628–8638, 2021. 1, 2, 6, 7
- [5] Yun-Chun Chen, Chen Gao, Esther Robb, and Jia-Bin Huang. Nas-dip: Learning deep image prior with neural architecture search. In *European Conference on Computer Vision*, pages 442–459. Springer, 2020. 3
- [6] Alexey Dosovitskiy, Lucas Beyer, Alexander Kolesnikov, Dirk Weissenborn, Xiaohua Zhai, Thomas Unterthiner, Mostafa Dehghani, Matthias Minderer, Georg Heigold, Sylvain Gelly, et al. An image is worth 16x16 words: Transformers for image recognition at scale. *arXiv preprint arXiv:2010.11929*, 2020. 2, 3
- [7] Rita Fermanian, Mikael Le Pendu, and Christine Guillemot. Regularizing the Deep Image Prior with a Learned Denoiser for Linear Inverse Problems. In *MMSP 2021 - IEEE 23rd International Workshop on Multimedia Signal Processing*, pages 1–6, Tampere, Finland, Oct. 2021. IEEE. 3
- [8] Yosef Gandelsman, Assaf Shocher, and Michal Irani. ”double-dip”: Unsupervised image decomposition via coupled deep-image-priors. In *Proceedings of the IEEE/CVF Conference on Computer Vision and Pattern Recognition*, pages 11026–11035, 2019. 1, 2, 6
- [9] Kuang Gong, Ciprian Catana, Jinyi Qi, and Quanzheng Li. Pet image reconstruction using deep image prior. *IEEE Transactions on Medical Imaging*, 38(7):1655–1665, 2019. 3
- [10] Kuang Gong, Ciprian Catana, Jinyi Qi, and Quanzheng Li. Direct reconstruction of linear parametric images from dynamic pet using nonlocal deep image prior. *IEEE Transactions on Medical Imaging*, 41(3):680–689, 2022. 3

- [11] Rana Hanocka, Gal Metzer, Raja Giryes, and Daniel Cohen-Or. Point2mesh: A self-prior for deformable meshes. *ACM Trans. Graph.*, 39(4), 2020. [1](#)
- [12] Fumio Hashimoto, Kibo Ote, and Yuya Onishi. PET image reconstruction incorporating deep image prior and a forward projection model. *IEEE Transactions on Radiation and Plasma Medical Sciences*, 6(8):841–846, nov 2022. [3](#)
- [13] Amir Hertz, Or Perel, Raja Giryes, Olga Sorkine-Hornung, and Daniel Cohen-Or. Sape: Spatially-adaptive progressive encoding for neural optimization. *Advances in Neural Information Processing Systems*, 34:8820–8832, 2021. [2](#), [8](#)
- [14] Edwin Kurniawan, Yunjin Park, and Sukho Lee. Noise-resistant demosaicing with deep image prior network and random rgbw color filter array. *Sensors*, 22(5):1767, 2022. [3](#)
- [15] Alexander Li and Deepak Pathak. Functional regularization for reinforcement learning via learned fourier features. *Advances in Neural Information Processing Systems*, 34:19046–19055, 2021. [2](#)
- [16] Yang Li, Si Si, Gang Li, Cho-Jui Hsieh, and Samy Bengio. Learnable fourier features for multi-dimensional spatial positional encoding. *Advances in Neural Information Processing Systems*, 34:15816–15829, 2021. [3](#)
- [17] David B. Lindell, Dave Van Veen, Jeong Joon Park, and Gordon Wetzstein. Bacon: Band-limited coordinate networks for multiscale scene representation. In *CVPR*, 2022. [2](#), [8](#)
- [18] Erika Lu, Forrester Cole, Tali Dekel, Andrew Zisserman, William T Freeman, and Michael Rubinstein. Omnimate: Associating objects and their effects in video. In *CVPR*, 2021. [3](#), [6](#)
- [19] Gary Mataev, Michael Elad, and Peyman Milanfar. Deepred: Deep image prior powered by red. *ArXiv*, abs/1903.10176, 2019. [3](#)
- [20] Ben Mildenhall, Peter Hedman, Ricardo Martin-Brualla, Pratul P Srinivasan, and Jonathan T Barron. Nerf in the dark: High dynamic range view synthesis from noisy raw images. In *Proceedings of the IEEE/CVF Conference on Computer Vision and Pattern Recognition*, pages 16190–16199, 2022. [1](#), [2](#), [8](#)
- [21] Himashi Peiris, Munawar Hayat, Zhaolin Chen, Gary Egan, and Mehrtash Harandi. A robust volumetric transformer for accurate 3d tumor segmentation. In *International Conference on Medical Image Computing and Computer-Assisted Intervention*, pages 162–172. Springer, 2022. [2](#)
- [22] Jordi Pont-Tuset, Federico Perazzi, Sergi Caelles, Pablo Arbeláez, Alex Sorkine-Hornung, and Luc Van Gool. The 2017 davis challenge on video object segmentation. *arXiv preprint arXiv:1704.00675*, 2017. [7](#)
- [23] Nasim Rahaman, Aristide Baratin, Devansh Arpit, Felix Draxler, Min Lin, Fred Hamprecht, Yoshua Bengio, and Aaron Courville. On the spectral bias of neural networks. In *International Conference on Machine Learning*, volume 97, pages 5301–5310, 2019. [2](#)
- [24] Dongwei Ren, Kai Zhang, Qilong Wang, Qinghua Hu, and Wangmeng Zuo. Neural blind deconvolution using deep priors. In *Proceedings of the IEEE/CVF Conference on Computer Vision and Pattern Recognition*, pages 3341–3350, 2020. [3](#)
- [25] Zenglin Shi, Pascal Mettes, Su bhransu Maji, and Cees G M Snoek. On measuring and controlling the spectral bias of the deep image prior. *International Journal of Computer Vision*, 2022. [1](#), [3](#), [6](#)
- [26] Vincent Sitzmann, Julien N.P. Martel, Alexander W. Bergman, David B. Lindell, and Gordon Wetzstein. Implicit neural representations with periodic activation functions. In *arXiv*, 2020. [2](#)
- [27] Matthew Tancik, Pratul P. Srinivasan, Ben Mildenhall, Sara Fridovich-Keil, Nithin Raghavan, Utkarsh Singhal, Ravi Ramamoorthi, Jonathan T. Barron, and Ren Ng. Fourier features let networks learn high frequency functions in low dimensional domains. *NeurIPS*, 2020. [2](#), [3](#)
- [28] Dmitry Ulyanov, Andrea Vedaldi, and Victor Lempitsky. Deep image prior. In *Proceedings of the IEEE conference on computer vision and pattern recognition*, pages 9446–9454, 2018. [1](#), [2](#), [3](#), [4](#), [12](#)
- [29] Ashish Vaswani, Noam Shazeer, Niki Parmar, Jakob Uszkoreit, Llion Jones, Aidan N Gomez, Łukasz Kaiser, and Illia Polosukhin. Attention is all you need. In I. Guyon, U. Von Luxburg, S. Bengio, H. Wallach, R. Fergus, S. Vishwanathan, and R. Garnett, editors, *Advances in Neural Information Processing Systems*, volume 30. Curran Associates, Inc., 2017. [2](#)
- [30] Hengkang Wang, Taihui Li, Zhong Zhuang, Tiancong Chen, Hengyue Liang, and Ju Sun. Early stopping for deep image prior, 2021. [3](#)
- [31] Rui Xu, Xintao Wang, Kai Chen, Bolei Zhou, and Chen Change Loy. Positional encoding as spatial inductive bias in gans, 2020. [2](#)
- [32] Tatsuya Yokota, Kazuya Kawai, Muneyuki Sakata, Yuichi Kimura, and Hidekata Hontani. Dynamic pet image reconstruction using nonnegative matrix factorization incorporated with deep image prior. In *Proceedings of the IEEE/CVF International Conference on Computer Vision (ICCV)*, October 2019. [3](#)
- [33] Jaejun Yoo, Kyong Hwan Jin, Harshit Gupta, Jerome Yerly, Matthias Stuber, and Michael Unser. Time-dependent deep image prior for dynamic mri. *IEEE Transactions on Medical Imaging*, 2021. [3](#), [4](#)
- [34] Kai Zeng and Zhou Wang. 3d-ssim for video quality assessment. In *2012 19th IEEE International Conference on Image Processing*, pages 621–624, 2012. [7](#)
- [35] Roman Zeyde, Michael Elad, and Matan Protter. On single image scale-up using sparse-representations. In *International conference on curves and surfaces*, pages 711–730. Springer, 2010. [4](#)
- [36] Haotian Zhang, Long Mai, Ning Xu, Zhaowen Wang, John Collomosse, and Hailin Jin. An internal learning approach to video inpainting. In *Proceedings of the IEEE/CVF International Conference on Computer Vision (ICCV)*, October 2019. [1](#), [3](#)
- [37] Jenny Zukerman, Tom Tirer, and Raja Giryes. Bp-dip: A backprojection based deep image prior. In *2020 28th European Signal Processing Conference (EUSIPCO)*, pages 675–679. IEEE, 2021. [3](#)

## A. Comparison to meshgrid

In the main paper we compared an MLP model with FF vs. meshgrid inputs. We showed meshgrid is unable to reach the FF performance in terms of PSNR. Here we additionally show a visual results when meshgrid is used as input (Figure 12). With meshgrid as input the results are over-smoothed and the model is unable to recover details.

## B. Image denoising

In this section we provide a detailed PSNR comparison of all the images in the standard dataset<sup>2</sup>. The full results for all images are in table 6.

## C. Image SR

We provide a detailed PSNR comparison between DIP and PIP along with visual examples. For PIP-CNN we changed the learning rate from 0.01 to 0.001 in both learned and fixed FF. The full quantitative results for  $\times 4$  SR are presented in Table 7 (Set5) and Table 8 (Set14). The full quantitative results for  $\times 8$  SR are presented in Table 9 (Set5) and Table 10 (Set14).

## D. Video denoising

We provide the generated videos as described in the paper. PIP produces higher temporal consistency and less blurry background compared to 2D-DIP (frame-by-frame) and 3D-DIP. All videos are available in [the project page](#), or the direct links below.

	Dog	Judo	Rollerblade	Camel
GT	<a href="#">dog_gt.mp4</a>	<a href="#">judo_gt.mp4</a>	<a href="#">rollerblade_gt.avi</a>	<a href="#">camel_gt.mp4</a>
Noisy	<a href="#">dog_noisy.mp4</a>	<a href="#">judo_noisy.mp4</a>	<a href="#">rollerblade_noisy.mp4</a>	<a href="#">camel_noisy.mp4</a>
2D-DIP	<a href="#">dog_dip.mp4</a>	<a href="#">judo_dip.mp4</a>	<a href="#">rollerblade_dip.mp4</a>	<a href="#">camel_dip.mp4</a>
3D-DIP	<a href="#">dog_d3_dip.mp4</a>	<a href="#">judo_d3_dip.mp4</a>	<a href="#">rollerblade_d3_dip.mp4</a>	<a href="#">camel_d3_dip.mp4</a>
PIP	<a href="#">dog_pip.mp4</a>	<a href="#">judo_pip.mp4</a>	<a href="#">rollerblade_pip.mp4</a>	<a href="#">camel_pip.mp4</a>

## E. Video Super-Resolution (SR)

We provide the generated videos as described in the paper. PIP produces higher temporal consistency and less blurry background compared to 2D-DIP (frame-by-frame) and 3D-DIP. All videos are available in [the project page](#), or the direct links below.

	Dog	Judo	Rollerblade	Camel
GT	<a href="#">dog_gt.mp4</a>	<a href="#">judo_gt.mp4</a>	<a href="#">rollerblade_gt.avi</a>	<a href="#">camel_gt.mp4</a>
LR	<a href="#">dog_lr.mp4</a>	<a href="#">judo_lr.mp4</a>	<a href="#">rollerblade_lr.mp4</a>	<a href="#">camel_lr.mp4</a>
2D-DIP	<a href="#">dog_dip.mp4</a>	<a href="#">judo_dip.mp4</a>	<a href="#">rollerblade_dip.mp4</a>	<a href="#">camel_dip.mp4</a>
3D-DIP	<a href="#">dog_d3_dip.mp4</a>	<a href="#">judo_d3_dip.mp4</a>	<a href="#">rollerblade_d3_dip.mp4</a>	<a href="#">camel_d3_dip.mp4</a>
PIP	<a href="#">dog_pip.mp4</a>	<a href="#">judo_pip.mp4</a>	<a href="#">rollerblade_pip.mp4</a>	<a href="#">camel_pip.mp4</a>

<sup>2</sup>[https://webpages.tuni.fi/foi/GCF-BM3D/index.html#ref\\_results](https://webpages.tuni.fi/foi/GCF-BM3D/index.html#ref_results)



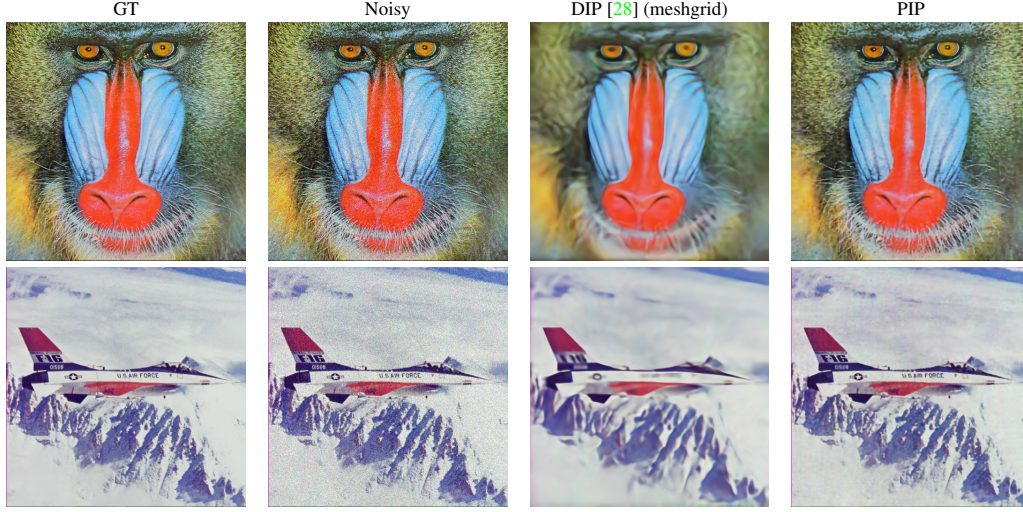


Figure 12. Image denoising ( $\sigma = 25$ ), comparison of PIP to DIP with meshgrid encoding

	Arch.	Freq.	Baboon	F16	House	Peppers	Lena	Kodim01	kodim02	kodim03	kodim12	Avg.
DIP	CNN	-	22	30.12	29.56	29.79	28.89	25.67	<b>30.19</b>	30.62	30.2	28.56
DIP	MLP	-	13.28	15.34	13.83	14.87	13.06	16.09	20.63	15.31	14.93	15.26
PIP	CNN	Fixed	22	<b>30.93</b>	<b>29.67</b>	<b>30.75</b>	28.97	<b>25.9</b>	30.11	30.42	30.43	<b>28.8</b>
PIP	CNN	Learned	<b>22.2</b>	30.2	29.35	29.54	29.3	25.31	29.72	<b>30.69</b>	30.23	28.28
PIP	MLP	Fixed	21.52	29.92	28.47	29.77	29.12	25.27	29.59	30.41	<b>30.48</b>	28.26
PIP	MLP	Learned	21.58	30.02	28.69	29.8	<b>29.35</b>	25.13	29.78	30.25	29.52	28.24

Table 6. Detailed denoising PSNR comparison for the “standard dataset” ( $\sigma = 25$ ). Note that replacing random encoding with a learned one both (i) improves performance and (ii) allows replacing the CNN with MLP. PIP with MLP is more efficient and has only minor degradation in reconstruction performance, unlike DIP with MLP.

	Arch.	Freq.	Baby	Bird	Butterfly	Head	Woman	Avg.
DIP	CNN	-	31.13	32.07	<b>26.74</b>	31.21	28.41	29.914
DIP	MLP	-	23.27	24.18	19.9	25.69	21.2	22.85
PIP	CNN	Fixed	<b>32.86</b>	32.01	25.95	31.37	<b>28.89</b>	30.22
PIP	CNN	Learned	32.77	<b>32.39</b>	26.28	31.66	28.6	<b>30.34</b>
PIP	MLP	Fixed	27.82	32.22	25.14	<b>31.96</b>	28.53	29.14
PIP	MLP	Learned	32.6	32.12	25.05	31.92	28.55	30.05

Table 7. Detailed super-resolution ( $\times 4$ ) PSNR comparison for the Set5 dataset. Note that replacing random encoding with Fourier Features in PIP both (i) improves performance and (ii) allows replacing the CNN with MLP. PIP with MLP is more efficient and has only minor degradation in reconstruction performance, unlike DIP with MLP.

	Arch.	Freq.	Baboon	Barbara	Bridge	Coastguard	Comic	Face	Flowers	Foreman	Lena	Man	Monarch	Peppers	Ppt3	Zebra	Avg.
DIP	CNN	-	22.46	25.46	23.22	25.67	22.34	31.02	26.47	31.66	30.17	26.15	30.17	31.98	24.19	25.76	26.95
DIP	MLP	-	20.13	21.21	18.9	22.79	19.11	25.34	20.74	23.66	23.59	20.52	21.71	22.97	16.93	19.63	21.23
PIP	CNN	Fixed	21.64	25.5	23.5	25.64	22.25	31.87	25.63	32.13	30.92	25.82	<b>30.86</b>	32.57	24.07	25.98	27.03
PIP	CNN	Learned	22.53	<b>25.59</b>	<b>23.62</b>	25.25	22.33	<b>31.91</b>	<b>26.59</b>	<b>32.29</b>	<b>31.41</b>	26.48	30.48	<b>32.7</b>	<b>24.68</b>	<b>26.1</b>	<b>27.78</b>
PIP	MLP	Fixed	<b>22.61</b>	25.48	23.46	<b>25.86</b>	<b>22.38</b>	31.77	26.57	31.57	30.44	<b>26.58</b>	28.3	32.38	24.26	25.76	26.96
PIP	MLP	Learned	22.59	25.49	23.5	25.82	22.28	<b>31.91</b>	26.55	31.64	31.16	26.53	29.59	32.41	24.12	25.81	27.1

Table 8. Detailed super-resolution ( $\times 4$ ) PSNR comparison for the Set14 dataset. Note that replacing random encoding with Fourier Features in PIP both (i) improves performance and (ii) allows replacing the CNN with MLP. PIP with MLP is more efficient and has only minor degradation in reconstruction performance, unlike DIP with MLP.



	Arch.	Freq.	Baby	Bird	Butterfly	Head	Woman	Avg.
DIP	CNN	-	28.15	<b>27.28</b>	<b>20.22</b>	<b>29.35</b>	<b>24.6</b>	<b>25.92</b>
DIP	MLP	-	16.82	17.82	13.74	18.96	14.64	16.4
PIP	CNN	Fixed	27.11	26.35	18.88	22.513	21.87	23.34
PIP	CNN	Learned	28.53	26.71	19.23	19.16	24.25	25.57
PIP	MLP	Fixed	28.2	25.97	18.77	28.45	23.03	24.88
PIP	MLP	Learned	<b>28.56</b>	26.76	19.36	29.29	24.48	25.69

Table 9. Detailed super-resolution ( $\times 8$ ) PSNR comparison for the Set5 dataset. Note that replacing random encoding with FF in PIP allows replacing the CNN with MLP. PIP with MLP is more efficient and has only minor degradation in reconstruction performance, unlike DIP with MLP.

	Arch.	Freq.	Baboon	Barbara	Bridge	Coastguard	Comic	Face	Flowers	Foreman	Lena	Man	Monarch	Peppers	Ppt3	Zebra	Avg.
DIP	CNN	-	<b>21.44</b>	<b>24.02</b>	21.03	<b>24.22</b>	<b>20.02</b>	<b>29.45</b>	<b>23.05</b>	27.39	<b>27.87</b>	23.78	24.94	<b>29.08</b>	20.16	<b>20.94</b>	<b>24.1</b>
DIP	MLP	-	18.17	17.57	15.75	20.01	14.66	18.96	16.51	17.25	18.63	16.55	17.96	17.36	13.5	16.06	17.07
PIP	CNN	Fixed	21.08	23.29	20.65	24.09	19.65	29.37	22.42	<b>28.76</b>	27.66	21.67	24.91	28.98	19.86	19.61	24
PIP	CNN	Learned	21.4	23.86	21.04	24.18	19.86	29.25	22.95	26.91	27.69	23.65	<b>25.11</b>	28.67	<b>20.31</b>	20.21	23.94
PIP	MLP	Fixed	21.25	23.86	20.62	23.76	19.69	28.39	22.75	26.23	27.53	23.46	24.52	28.57	19.98	20.25	23.63
PIP	MLP	Learned	21.42	23.9	<b>21.11</b>	24.16	19.64	29.2	22.91	27.15	27.7	<b>23.81</b>	24.53	28.51	20.05	20.38	23.89

Table 10. Detailed super-resolution ( $\times 8$ ) PSNR comparison for the Set14 dataset. Note that replacing random encoding with FF in PIP allows replacing the CNN with MLP. PIP with MLP is more efficient and has only minor degradation in reconstruction performance, unlike DIP with MLP.